

# EEG-Based Emotion Recognition Using Regularized Graph Neural Networks

Peixiang Zhong, Di Wang, and Chunyan Miao,

**Abstract**—In this paper, we propose a regularized graph neural network (RGNN) for EEG-based emotion recognition. EEG signals measure the neuronal activities on different brain regions via electrodes attached on them. Existing studies do not exploit the topological structure of EEG signals effectively. Our RGNN model is biologically supported and captures both local and global inter-channel relations. In addition, we propose two regularizers, namely NodeDAT and EmotionDL, to improve the robustness of our model against cross-subject EEG variations and noisy labels during recording. To thoroughly evaluate our model, we conduct extensive experiment in both subject-dependent and subject-independent classification settings on two public datasets SEED and SEED-IV. Our model obtains better performance than a few competitive baselines such as SVM, DBN, DGCNN, BiDANN, and the state-of-the-art BiHDM on most of the tasks. Our model analysis demonstrates that our proposed biologically-supported adjacency matrix and two regularizers contribute consistent and significant gain to the performance of our model. Investigations on the neuronal activities reveal that pre-frontal, parietal and occipital regions may be the most informative regions in emotion recognition. In addition, local inter-channel relations between (FP1, AF3), (F6, F8) and (FP2, AF4) may provide useful information as well.

**Index Terms**—Affective Computing, EEG, Graph Neural Network

arXiv:1907.07835v1 [cs.CV] 18 Jul 2019

## 1 INTRODUCTION

**E**MOTION recognition is an important subarea of affective computing, which focuses on recognizing human emotions based on a variety of modalities such as audio-visual expressions, body language and physiological signals. Compared to other modalities, physiological signals such as electroencephalogram (EEG), electrocardiogram (ECG), electromyogram (EMG), and galvanic skin response (GSR), etc. have the advantage of being difficult to hide or disguise. In recent years, due to the rapid development of noninvasive, easy-to-use and inexpensive EEG recording devices, EEG-based emotion recognition has received increasing attention in both research [1] and applications [2].

Emotion models can be broadly categorized into discrete models and dimensional models. The former categorizes emotions into discrete entities, e.g., anger, disgust, fear, happiness, sadness, and surprise in Ekman’s theory [3]. The latter describes emotions using their underlying dimensions, e.g., valence, arousal and dominance [4], which measures emotions from unpleasant to pleasant, passive to active, and submissive to dominant, respectively.

EEG signals measures voltage fluctuations from the cortex in the brain and have been shown to reveal important information about human emotional states [5]. For example, greater relative left frontal EEG activity has been observed when experiencing positive emotions. The voltage fluctuations on different brain regions are measured by electrodes attached on the scalp. Each electrode refers to one channel in the EEG signals. The collected EEG signals are often analyzed in specific frequency bands for each channel: delta (1-4 Hz), theta (4-7 Hz), alpha (8-13 Hz), beta (13-30 Hz),

and gamma ( $>30$  Hz).

Existing EEG-based emotion recognition methods are primarily based the supervised machine learning approach where features are extracted from preprocessed EEG signals in each channel over a time window and then a classifier is trained on the extracted features to recognize emotions. Wang *et al.* [6] compared power spectral density features (PSD), wavelet features and nonlinear dynamical features with a Support Vector Machine (SVM) classifier. Zheng and Lu [7] investigated critical frequency bands and channels using PSD, differential entropy (DE) [8] and PSD asymmetry features, and obtained robust accuracy using deep belief networks (DBN). However, most existing EEG-based emotion recognition approaches do not address the following drawbacks: 1) The topological structure of EEG signals are not effectively exploited to learn more discriminative EEG representations. 2) EEG signals vary significantly across different subjects, which hinders the generalizability of trained classifiers. 3) Participants may not always generate the intended emotions when watching emotion-eliciting movie clips. Consequently, the emotion labels in the EEG data are noisy and may not reflect the true elicited emotions.

There are several attempts to address the first two drawbacks. Zhang *et al.* [9] and Zhang *et al.* [10] incorporated spatial relations in EEG signals using convolutional neural networks (CNN) and recurrent neural networks (RNN), respectively. However, their approach require a 2D representation of EEG channels on the scalp, which may cause information loss during flattening because channels are arranged in a 3D space. In addition, their approach of using CNNs and RNNs to capture inter-channel relations has difficulty in learning long-range dependencies [11]. Graph neural networks (GNN) are proposed in [12] to capture inter-channel relations using an adjacency matrix. However, similar to CNNs and RNNs, their approach only considers

• *P. Zhong, D. Wang and C. Miao are with the School of Computer Science and Engineering, Nanyang Technological University, Singapore. E-mail: peixiang001@e.ntu.edu.sg*

*Manuscript received April 19, 2019; revised August 26, 2019.*

relations between nearest channels, which thus may loss valuable information between distant channels, such as PSD asymmetry between channels on the left and right hemispheres in the frontal region, which is informative in valence prediction [5]. A very recent work [13] applies RNNs to learn EEG representations in the two hemispheres separately and then adopts the asymmetric differences between them to recognize emotions. However, their final classification is limited to the bi-hemispherical discrepancies and ignores other useful features such as neuronal activities on each channel.

In recent years, several studies [14], [15] investigated the transferability of EEG-based emotion recognition models across subjects. Lan *et al.* [16] compared several domain adaptation techniques such as maximum independence domain adaptation (MIDA), transfer component analysis (TCA), and subspace alignment (SA), etc., and found that they can improve subject-independent classification accuracy by around 10%. Li *et al.* [17] applied domain adversarial learning to lower the influence of individual subject on EEG data and obtained improved performance as well.

In this paper, we propose a regularized graph neural network (RGNN) that addresses all three aforementioned drawbacks together. Specifically, our RGNN model leverages the topological structure of EEG signals, i.e., according to the economy of brain network organization [18], we extends the simple graph convolution network (SGC) [19] and propose a biologically-supported sparse adjacency matrix to capture both local and global inter-channel relations. Local inter-channel relations may reveal anatomical connectivity patterns and help alleviate the EEG measurement confounds caused by volume conduction. Global inter-channel relations may reveal functional connectivity patterns across different hemispheres and provide valuable emotion-related asymmetry information. In addition, we propose a node-wise domain adversarial training (NodeDAT) to regularize our graph model such that it generalizes better to subject-independent classification scenarios. Different from the domain adversarial training in [17], [20], our NodeDAT regularizes the domain discrepancies between features in each channel in the source and target domains. Finally, we propose an emotion-aware distribution learning (EmotionDL) method to address the problem of noisy labels during training. Studies have shown that noisy labels can adversely impact classification accuracy [21]. Instead of learning single-label classification, our EmotionDL learns a distribution of labels during training and thus acts as a regularizer to improve the robustness of our model against noisy labels.

In summary, the main contributions of this paper are as follows:

- We propose a regularized graph neural network (RGNN) model to recognize emotions based on EEG signals. Our model is biologically supported and captures local and global inter-channel relations.
- We propose two regularizers: a node-wise domain adversarial training (NodeDAT) and an emotion-aware distribution learning (EmotionDL). NodeDAT improves our subject-independent recognition performance. EmotionDL improves the robustness of

our model against noisy labels.

- We conduct extensive experiment in both subject-dependent and subject-independent classification settings on two public EEG datasets with pre-computed features, namely SEED [7] and SEED-IV [22]. Experimental results demonstrate the effectiveness of our proposed model and regularizers. In addition, our RGNN achieves superior performance over the state-of-the-art baselines on most of the tasks.
- Investigations on the neuronal activities reveal that pre-frontal, parietal and occipital regions may be the most informative regions in emotion recognition. In addition, local inter-channel relations between (FP1, AF3), (F6, F8) and (FP2, AF4) may provide useful information as well.

## 2 RELATED WORK

### 2.1 EEG-Based Emotion Recognition

EEG features and classifiers are the two fundamental components in the machine learning approach of EEG-based emotion recognition. EEG features can be broadly divided into single-channel features and multi-channel features. The majority of existing features is single-channel features such as statistical features [23], Hjorth features [24], fractal dimension (FD) [25], PSD, differential entropy (DE) [8], and wavelet features [26]. A more detailed comparison of EEG features is discussed in [27]. A few features are computed on multiple channels to capture the inter-channel relations, e.g., the asymmetry features of PSD [7] and functional connectivity patterns [28], [29], where common indices such as correlation, coherence and phase synchronization were used estimate brain functional connectivity between channels. However, their approaches require labor-intensive manual connectivity analysis for each subject and may not be ideal for real-time applications.

Similarly, EEG classifiers can be broadly divided into topology-invariant classifiers and topology-aware classifiers. The majority of existing classifiers are topology-invariant classifiers such as SVM, k-Nearest Neighbors (KNN), DBNs [30] and RNNs [31], which do not take the topological structure of EEG features into account when learning the EEG representations. By contrast, topology-aware classifiers such as CNNs in [9], [32], [33], [34] and GNNs in [12] consider the inter-channel topological relations and learn EEG representations for each channel by aggregating features from nearby channels using convolutional operations in either the Euclidean space or the non-Euclidean space. However, as discussed in Section 1, existing CNNs and GNNs have difficulty learning the dependencies between distant channels which may reveal important emotion-related information. Recently, Zhang *et al.* [10] and Li *et al.* [13] proposed to use RNNs to learn spatial topological relations between channels by scanning electrodes in both vertical and horizontal directions. However, their approaches do not fully exploit the topological structure of channels on the scalp. For example, two topologically close channels may be far away from each other in the scanning sequence.

## 2.2 Graph Neural Networks

Graph neural networks (GNN) is a class of neural networks dealing with data in the graph domains, e.g., molecular structures, social networks and knowledge graphs [35]. The early work [36] on GNNs aim to learn a converged static state embedding for each node in the graph using a transition function applied to its neighborhood. Later, inspired by the convolutional operation of CNN in Euclidean domains, Bruna *et al.* [37] combined spectral graph theory [38] with neural networks and defined convolutional operations in graph domains using the spectral filters computed from the (normalized) graph Laplacian. Following this line of research, Defferrard *et al.* [39] proposed fast localized convolutions by using a recursive formulation of the  $K$ -order Chebyshev polynomials to approximate the filters. The resulted representation for each node is an aggregation of its  $K^{\text{th}}$ -order neighborhood. Kipf and Welling [40] limited  $K = 1$  and proposed the standard graph convolutional networks (GCN) with a faster localized graph convolutional operation. The convolutional layers in GCN can be stacked  $K$  times to effectively convolve the  $K^{\text{th}}$ -order neighborhood of a node. Recently, Wu *et al.* [19] further simplified GCN by removing the nonlinearities between convolutional layers in GCN and proposed the simple graph convolution networks (SGC), which effectively behaves like a linear feature transformation followed by a logistic regression. SGC has been demonstrated to perform orders of magnitude faster than GCNs with comparable classification accuracy.

Apart from GCNs, there are other variants of GNNs. Velikovi *et al.* [41] proposed graph attention networks (GAT) to aggregate neighboring nodes using weights computed by masked self-attention [42]. Li *et al.* [43] proposed gated graph neural network (GGNN) to aggregate neighboring nodes using gated recurrent units (GRU) [44] to improve the long-term propagation of information. More detailed comparisons for GNNs are discussed in [35], [45].

## 2.3 Unsupervised Domain Adaptation

Unsupervised domain adaptation aims to mitigate the domain shift when transferring knowledge from a supervised source domain to an unsupervised target domain. The most common approaches are instance re-weighting, domain-invariant feature learning, domain mapping and normalization statistics. Instance re-weighting methods [46] aims to infer the resampling weight directly by feature distribution matching across source and target domains in a non-parametric manner. Domain-invariant feature learning methods align features from both source and target domains to a common feature space. The alignment can be achieved by minimizing divergence [47], maximizing reconstruction [48] or adversarial training [20]. The domain mapping technique is typically applied in the computer vision field where pixel-level image-to-image translation from one domain to another domain improves domain adaptation performance [49]. Normalization statistics is based on the assumption that the batch norm statistics learn domain knowledge. Cariucci *et al.* [50] performed domain adaptation by modulating the batch norm layers' statistics from source to target domain. More methods on unsupervised domain adaptation are discussed in [51], [52].

## 2.4 Learning with Noisy Labels

Common approaches to learning with noisy labels are based on the noise transition matrix and robust loss functions. The noise transition matrix specifies the probabilities of transition from each ground true label to each noisy label and is often applied to modify the cross-entropy loss. The matrix can be pre-computed as a prior [53] or estimated from noisy data [54]. A few studies tackle noisy labels by using noise-tolerant robust loss functions, such as unhinged loss [55] and ramp loss [56]. Several other approaches include bootstrap that leverages predicted labels to generate training targets [57] and alternatively updating network parameters and labels during training [58]. Our EmotionDL is most related to [59], which applies distribution learning to learn labels with ambiguity in the computer vision domain.

## 3 PRELIMINARY

In this section, we introduce the preliminaries for simple graph convolution networks (SGC) [19] and its spectral analysis, which is the basis for our RGNN model.

### 3.1 Simple Graph Convolution Networks (SGC)

Given a graph  $\mathcal{G} = (\mathcal{V}, \mathcal{E})$ , where  $\mathcal{V}$  denotes a set of nodes and  $\mathcal{E}$  denotes a set of edges between nodes in  $\mathcal{V}$ . Data on  $\mathcal{V}$  can be represented by a feature matrix  $\mathbf{X} \in \mathbb{R}^{n \times d}$ , where  $n$  denotes the number of nodes and  $d$  denotes the input feature dimension. The edge set  $\mathcal{E}$  can be represented by a weighted adjacency matrix  $\mathbf{A} \in \mathbb{R}^{n \times n}$  with self-loops, i.e.,  $\mathbf{A}_{ii} = 1$ ,  $i = 1, 2, \dots, n$ . In general, GNNs learn a feature transformation function for  $\mathbf{X}$  and produces output  $\mathbf{Z} \in \mathbb{R}^{n \times d'}$ , where  $d'$  denotes the output feature dimension.

Between layers in GNNs, the feature transformation can be written as

$$\mathbf{H}^{l+1} = f(\mathbf{H}^l, \mathbf{A}) \quad (1)$$

where  $l = 0, 1, \dots, L - 1$ ,  $L$  denotes the number of layers,  $\mathbf{H}^0 = \mathbf{X}$ ,  $\mathbf{H}^L = \mathbf{Z}$ , and  $f$  denotes the function we want to learn. A simple  $f$  would be

$$f(\mathbf{H}^{l+1}) = \sigma(\mathbf{A}\mathbf{H}^l\mathbf{W}^l) \quad (2)$$

where  $\sigma$  denotes a non-linear function and  $\mathbf{W}^l$  denotes a weight matrix at layer  $l$ . For each node  $\mathbf{x}$ , this  $f$  simply sums up all node features in its neighborhood including  $\mathbf{x}$  itself, followed by a non-linear transformation. However, one major limitation of  $f$  is that repeatedly applying  $f$  along multiple layers may lead to  $\mathbf{H}^l$  with overly large values due to the sum operation. Kipf and Welling [40] alleviated this limitation by proposing the graph convolution network (GCN) as follows:

$$f(\mathbf{H}^{l+1}) = \sigma(\mathbf{D}^{-\frac{1}{2}}\mathbf{A}\mathbf{D}^{\frac{1}{2}}\mathbf{H}^l\mathbf{W}^l) \quad (3)$$

where  $\mathbf{D}$  denotes the diagonal degree matrix of  $\mathbf{A}$ , i.e.,  $\mathbf{D}_{ii} = \sum_j \mathbf{A}_{ij}$ . The normalized adjacency matrix  $\mathbf{D}^{-\frac{1}{2}}\mathbf{A}\mathbf{D}^{\frac{1}{2}}$  prevents  $\mathbf{H}$  from growing overly large. If we ignore  $\sigma$  and  $\mathbf{W}^l$  temporarily and expand (3), the hidden state  $\mathbf{H}_i^{l+1}$  for node  $\mathbf{x}_i$ ,  $i = 1, 2, \dots, n$ , is computed via

$$\mathbf{H}_i^{l+1} \leftarrow \frac{1}{\mathbf{D}_{ii} + 1} \mathbf{H}_i^l + \sum_{j=1}^n \frac{\mathbf{A}_{ij}}{\sqrt{(\mathbf{D}_{ii} + 1)(\mathbf{D}_{jj} + 1)}} \mathbf{H}_j^l \quad (4)$$

Note that each neighboring  $\mathbf{H}_j^l$  is now normalized by both the degree of  $\mathbf{x}_i$  and degree of  $\mathbf{x}_j$ . Essentially, for each node, the feature transformation function  $f$  in GCN is a non-linear transformation of the weighted sum of node features of itself and its neighborhood. Successively applying  $L$  graph convolutional layers aggregates node features within a neighborhood of size  $L$ .

To further accelerate training while keeping comparable performance, Wu *et al.* [19] removed the non-linear function  $\sigma$  in (3) and reparameterized all linear transformations  $\mathbf{W}^l$  across all layers into one linear transformation  $\mathbf{W}$  as follows:

$$\mathbf{Z} = \mathbf{H}^L = \mathbf{S} \mathbf{H}^{L-1} \mathbf{W}^{L-1} = \dots = \mathbf{S}^L \mathbf{X} \mathbf{W} \quad (5)$$

where  $\mathbf{S} = \mathbf{D}^{-\frac{1}{2}} \mathbf{A} \mathbf{D}^{\frac{1}{2}}$ , and  $\mathbf{W} = \mathbf{W}^{L-1} \mathbf{W}^{L-2} \dots \mathbf{W}^0$ . Essentially, SGC computes a topology-aware linear transformation  $\hat{\mathbf{X}} = \mathbf{S}^L \mathbf{X}$ , followed by one final linear transformation  $\mathbf{Z} = \hat{\mathbf{X}} \mathbf{W}$  before softmax operation.

### 3.2 Spectral Graph Convolution

We analyze GCN from the perspective of spectral graph theory [38]. Graph Fourier analysis relies on the graph Laplacian  $\mathbf{L} = \mathbf{D} - \mathbf{A}$  or the normalized graph Laplacian  $\hat{\mathbf{L}} = \mathbf{I} - \mathbf{D}^{-\frac{1}{2}} \mathbf{A} \mathbf{D}^{\frac{1}{2}}$ . Since  $\hat{\mathbf{L}}$  is a symmetric positive semidefinite matrix, it can be decomposed as  $\hat{\mathbf{L}} = \mathbf{U} \Lambda \mathbf{U}^T$ , where  $\mathbf{U}$  is the orthonormal eigenvector matrix of  $\hat{\mathbf{L}}$  and  $\Lambda = \text{diag}(\lambda_1, \dots, \lambda_N)$  is the diagonal matrix of corresponding eigenvalues. Given graph data  $\mathbf{X}$ , the graph Fourier transform of  $\mathbf{X}$  is  $\hat{\mathbf{X}} = \mathbf{U}^T \mathbf{X}$ . The inverse Fourier transform of  $\hat{\mathbf{X}}$  is  $\mathbf{X} = \mathbf{U} \hat{\mathbf{X}}$ . Hence, the graph convolution between  $\mathbf{X}$  and a filter  $\mathbf{G}$  is

$$\mathbf{X} * \mathbf{G} = \mathbf{U}((\mathbf{U}^T \mathbf{G}) \odot (\mathbf{U}^T \mathbf{X})) = \mathbf{U} \hat{\mathbf{G}} \mathbf{U}^T \mathbf{X} \quad (6)$$

where  $\odot$  denotes the Hammond product, and  $\hat{\mathbf{G}} = \text{diag}(\hat{g}_1, \dots, \hat{g}_N)$  denotes a diagonal matrix with  $n$  spectral filter coefficients.

To reduce the current learning complexity of  $\mathcal{O}(n)$  to the learning complexity of conventional CNN, i.e.,  $\mathcal{O}(K)$ , (6) can be approximated using the  $K$ -th order polynomials

$$\mathbf{U} \hat{\mathbf{G}} \mathbf{U}^T \mathbf{X} \approx \mathbf{U} \left( \sum_{i=0}^K \theta_i \Lambda^i \right) \mathbf{U}^T \mathbf{X} = \sum_{i=0}^K \theta_i \hat{\mathbf{L}}^i \mathbf{X} \quad (7)$$

where  $\theta_i$  denotes coefficients. To further reduce computational cost, [39] proposed to use Chebyshev polynomials to approximate the filtering operation as follows

$$\mathbf{U} \hat{\mathbf{G}} \mathbf{U}^T \mathbf{X} = \sum_{i=0}^K \theta_i T_i(\hat{\mathbf{L}}') \mathbf{X} \quad (8)$$

where  $\theta_i$  denotes learnable parameters,  $\hat{\mathbf{L}}'$  denotes the scaled normalized Laplacian  $\hat{\mathbf{L}}' = \frac{2}{\lambda_{\max}} \hat{\mathbf{L}} - \mathbf{I}$  with its eigenvalues lying within  $[-1, 1]$ , and  $T_i(x)$  denotes the Chebyshev polynomials recursively defined as  $T_i(x) = 2xT_{i-1}(x) - T_{i-2}(x)$  with  $T_0(x) = 1$  and  $T_1(x) = x$ .

The GCN proposed in [40] made a few approximations to simplify the filtering operation in (8): 1) use  $K = 1$ ; 2) set  $\lambda_{\max} = 2$ ; 3) set  $\theta_0 = -\theta_1$ . The resulted GCN arrives at (3). Essentially, the graph convolutional operations defined in (3) and (5) behave like a low-pass filter by smoothing the features of each node on the graph using node features in its neighborhood.

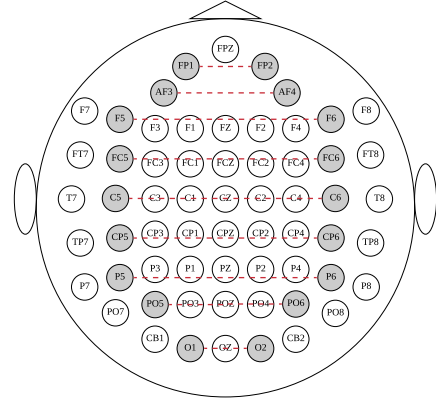


Fig. 1: The 62-channel EEG placement in SEED and SEED-IV. Gray symmetric channels are connected globally via red dashed lines.

## 4 OUR RGNN MODEL

In this section we present our approaches to constructing the biologically-supported adjacency matrix, and our RGNN model with two regularizers, i.e., NodeDAT and EmotionDL. The architecture of our model is illustrated in Figure 2.

### 4.1 Adjacency Matrix

The adjacency matrix  $\mathbf{A} \in \mathbb{R}^{n \times n}$  in RGNN represents the topological structure of channels on the scalp, where  $n$  denotes the number of channels. Each entry  $\mathbf{A}_{ij}$  in the adjacency matrix indicates the weight of connection between channels  $i$  and  $j$ . Note that  $\mathbf{A}$  contains self-loops. To reduce overfitting, we model  $\mathbf{A}$  as a symmetric matrix by using only  $\frac{n(n+1)}{2}$  parameters instead of  $n^2$ . Salvador *et al.* [60] observed that the strength of functional connectivity between brain regions decays as an inverse square or gravity-law function of physical distance. Hence, we initialize our adjacency matrix as follows

$$\mathbf{A}_{ij} = \exp\left(-\frac{d_{ij}}{2\delta^2}\right) \quad (9)$$

where  $d_{ij}$ ,  $i, j = 1, 2, \dots, n$ , denotes the physical distance between channels  $i$  and  $j$ , calculated from the data sheet of the recording device, and  $\delta$  denotes a sparsity hyperparameter controlling the decay rate of the functional connectivity between channels.

Bullmore and Sporns [18] proposed that the brain organization is shaped by an economic trade-off between minimizing wiring costs and network running costs. Minimizing wiring costs encourages local inter-channel connections as modelled in (9). However, minimizing network running costs encourages certain global inter-channel connections for high efficiency of information transfer across the network as a whole. To this end, we add a few global connections to the adjacency matrix. The global connections are subject to the specific EEG channel placement in the experiments. Figure 1 depicts the global connections in both SEED [7] and SEED-IV [22]. The selection of global channels is supported by the prior studies showing that the asymmetry in neuronal activities between left and right hemispheres

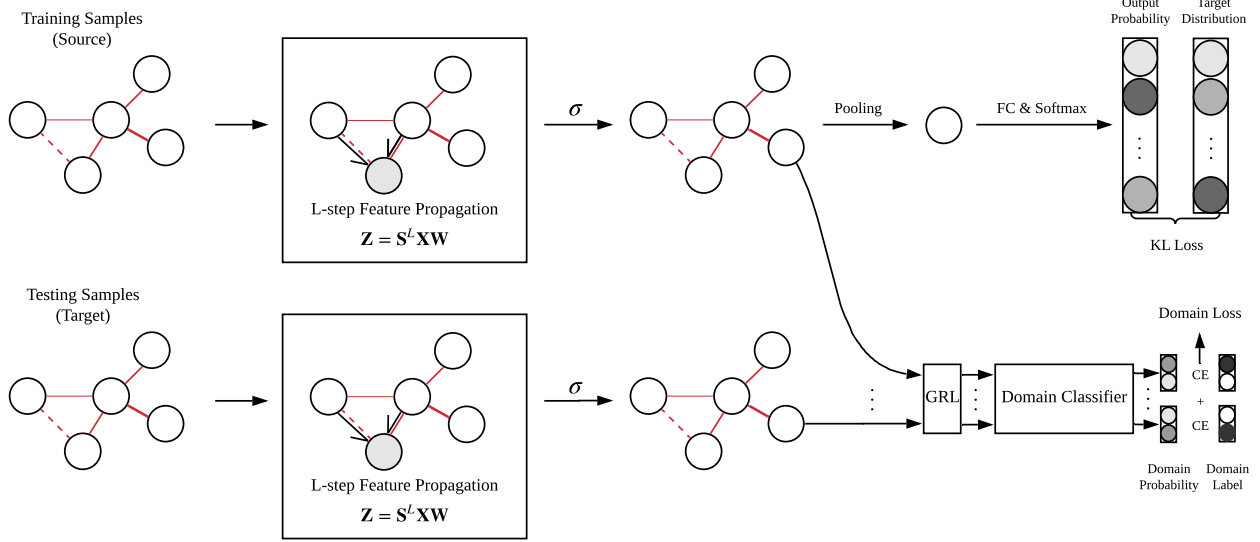


Fig. 2: The overall architecture of our RGNN model. FC denotes a fully-connected layer. CE denotes cross-entropy loss.

is informative in valence and arousal predictions [5], [61], [62]. To leverage the differential asymmetry information, we update  $\mathbf{A}$  as follows

$$\mathbf{A}_{ij} = \mathbf{A}_{ij} - 1 \quad (10)$$

where  $(i, j)$  denotes the indices of symmetric channel pairs: (FP1, FP2), (AF3, AF4), (F5, F6), (FC5, FC6), (C5, C6), (CP5, CP6), (P5, P6), (PO5, PO6), and (O1, O2). Note that our adjacency matrix  $\mathbf{A}$  in (10) effectively represents the brain network which combines both local anatomical connectivity and emotion-related global functional connectivity.

The last step in constructing the adjacency matrix is finding an optimal value of  $\delta$  to regularize the weights of connections between local channels. Achard and Bullmore [63] observed that sparse fMRI networks, comprising around 20% of all possible connections, typically maximize the efficiency of the network topology. Thus, we choose  $\delta$  such that around 20% of entries in  $\mathbf{A}$  are larger than 0.1 in absolute values. We empirically pick 0.1 as the threshold of having negligible connections between channels.

## 4.2 RGNN

Our RGNN model extends the SGC model [19]. Given EEG features  $\mathbf{X} \in \mathbb{R}^{N \times n \times d}$  and labels  $\mathbf{Y} \in \mathbb{Z}^N$ , where  $N$  denotes the number of training samples,  $n$  denotes the number of nodes or channels,  $d$  denotes the input feature dimension,  $\mathbf{Y}_i \in \{0, 1, \dots, C-1\}$  denotes the label index, and  $C$  denotes the number of classes. Our model aims to minimize the following cross-entropy loss

$$\Phi = - \sum_{i=1}^N \log(p(\mathbf{Y}_i | \mathbf{X}_i, \theta)) + \alpha \|\mathbf{A}\|_1 \quad (11)$$

where  $\theta$  denotes the model parameters we want to optimize, and  $\alpha$  denotes the L1 sparse regularization strength of our adjacency matrix  $\mathbf{A}$ .

By passing each feature matrix  $\mathbf{X}_i$  into our RGNN, the output probability of class  $\mathbf{Y}_i$  can be computed as

$$\begin{aligned} \mathbf{Z}_i &= \mathbf{S}^L \mathbf{X}_i \mathbf{W} \\ p(\mathbf{Y}_i | \mathbf{X}_i, \theta) &= \text{softmax}_i(\text{pool}(\sigma(\mathbf{Z}_i)) \mathbf{W}^O) \end{aligned} \quad (12)$$

where  $\mathbf{S} \in \mathbb{R}^{n \times n}$ ,  $\mathbf{W} \in \mathbb{R}^{d \times d'}$  and  $L$  follow the definitions in (5),  $\sigma(x) = \max(0, x)$  denotes the ReLU non-linear function,  $\mathbf{W}^O \in \mathbb{R}^{d' \times C}$  denotes the output weight matrix, and  $\text{pool}(\cdot)$  denotes the sum pooling across all nodes on the graph. We choose sum pooling because it demonstrated more expressive power than mean pooling and max pooling [64]. Note that we use the absolute values of  $\mathbf{A}$  to compute the degree matrix  $\mathbf{D}$  because  $\mathbf{A}$  has negative elements, i.e., global connections.

### 4.2.1 NodeDAT

EEG signals vary significantly across different subjects, which hinders the generalizability of trained classifiers. To improve subject-independent classification performance, we extend the domain adversarial training [20] by proposing a node-wise domain adversarial training (NodeDAT) to reduce the discrepancies between source and target domains, i.e., training and testing sets, respectively. Specifically, a domain classifier is proposed to classify each node representation into either source domain or target domain. Compared to [20], which only regularizes the pooled representation in the last layer, our NodeDAT has stronger regularization effect because it explicitly regularizes each node representation before pooling, as discussed in Section 6.2.1. During optimization, our model aims to confuse the domain classifier by learning domain-invariant representations for each node.

Specifically, given source data  $\mathbf{X} \in \mathbb{R}^{N \times n \times d}$  and unlabelled target data  $\mathbf{X}^T \in \mathbb{R}^{N \times n \times d}$ , where in practice  $\mathbf{X}^T$  can be either oversampled or downsampled to have the

same number of samples as  $\mathbf{X}$ , the domain classifier aims to minimize the following two binary cross-entropy losses

$$\Phi_D = - \sum_{i=1}^N \sum_{j=1}^n (\log(p_D(0|\mathbf{X}_i) + \log(p_D(1|\mathbf{X}_i^T)_j)) \quad (13)$$

where 0 and 1 denote source and target domains, respectively. The domain probabilities  $p_D(\cdot)_j$  for node  $j$  are computed as

$$\begin{aligned} p_D(0|\mathbf{X}_i)_j &= \text{softmax}_0(\sigma(\mathbf{Z}_{ij})\mathbf{W}^D) \\ p_D(1|\mathbf{X}_i^T)_j &= \text{softmax}_1(\sigma(\mathbf{Z}_{ij}^T)\mathbf{W}^D) \end{aligned} \quad (14)$$

where  $\mathbf{Z}_{ij}^{\{,T\}}$  denotes the  $j$ th node representation in  $\mathbf{Z}_i^{\{,T\}}$ , and  $\mathbf{W}^D \in \mathbb{R}^{d' \times 2}$  denotes the model parameters in the domain classifier.

Note that our domain classifier implements a gradient reversal layer (GRL) [20] to reverse the gradients of the domain classifier during backpropagation. The gradients are further scaled by a GRL scaling factor  $\beta$  which gradually increases from 0 to 1 as the training progresses. The gradually increasing  $\beta$  allows our domain classifier to be less sensitive to noisy inputs at the early stages of the training process. Specifically, as suggested in [20], we let  $\beta = \frac{2}{1+e^{-10p}} - 1$ , where  $p \in [0, 1]$  denotes the training progress.

#### 4.2.2 EmotionDL

Participants may not always generate the intended emotions when watching emotion-eliciting movie clips. To address the problem of noisy emotion labels in the datasets, we propose an emotion-aware distribution learning method (EmotionDL) to learn a distribution of classes instead of one single class for each training sample. Specifically, we convert each training label  $\mathbf{Y}_i \in \{0, 1, \dots, C-1\}$  into a prior probability distribution of all classes  $\hat{\mathbf{Y}}_i \in \mathbb{R}^C$ , where  $\hat{\mathbf{Y}}_{ic}$  denotes the probability of class  $c$  in  $\hat{\mathbf{Y}}_i$ . The conversion is dataset-dependent. In SEED, there are three classes: negative, neutral, and positive with corresponding class indices 0, 1, and 2, respectively. We convert  $\mathbf{Y}$  as follows

$$\hat{\mathbf{Y}}_i = \begin{cases} (1 - 2\epsilon/3, 2\epsilon/3, 0) & \mathbf{Y}_i = 0 \\ (\epsilon/3, 1 - 2\epsilon/3, \epsilon/3) & \mathbf{Y}_i = 1 \\ (0, 2\epsilon/3, 1 - 2\epsilon/3) & \mathbf{Y}_i = 2 \end{cases} \quad (15)$$

where  $\epsilon \in [0, 1]$  denotes a hyper-parameter controlling the noise level in the training labels. The converted class distribution centers on the original class and has non-zero probabilities at its nearest classes. This conversion mechanism is based on our assumption that participants are unlikely to generate opposite emotions when watching emotion-eliciting movie clips.

In SEED-IV, there are four classes: neutral, sad, fear, and happy with corresponding class indices 0, 1, 2, and 3, respectively. Similarly, we can convert  $\mathbf{Y}$  as follows

$$\hat{\mathbf{Y}}_i = \begin{cases} (1 - 3\epsilon/4, \epsilon/4, \epsilon/4, \epsilon/4) & \mathbf{Y}_i = 0 \\ (\epsilon/3, 1 - 2\epsilon/3, \epsilon/3, 0) & \mathbf{Y}_i = 1 \\ (\epsilon/4, \epsilon/4, 1 - 3\epsilon/4, \epsilon/4) & \mathbf{Y}_i = 2 \\ (\epsilon/3, 0, \epsilon/3, 1 - 2\epsilon/3) & \mathbf{Y}_i = 3 \end{cases} \quad (16)$$

The intuition behind this conversion is based on the distances between the four emotions on the valence-arousal

plane. Specifically, in the self-reported ratings [22], neutral, sad, fear, and happy movie ratings cluster in the zero valence zero arousal, negative valence negative arousal, negative valence positive arousal, and positive valence positive arousal regions, respectively. Thus, we assume that participants are likely to generate emotions that are have similar ratings in either valence or arousal dimensions, but unlikely to generate emotions that are far away in both dimensions, i.e., sad and happy.

After obtaining the converted class distributions  $\hat{\mathbf{Y}}$ , our model can be optimized by minimizing the following Kullback-Leibler (KL) divergence [65] instead of (11)

$$\Phi' = \sum_{i=1}^N \text{KL}(p(\mathbf{Y}|\mathbf{X}_i, \theta), \hat{\mathbf{Y}}_i) + \alpha \|\mathbf{A}\|_1 \quad (17)$$

where  $p(\mathbf{Y}|\mathbf{X}_i, \theta)$  denotes the output probability distribution computed via (12).

#### 4.2.3 Optimization

Combining NodeDAT and EmotionDL, the overall loss function of RGNN is as follows

$$\Phi'' = \Phi' + \Phi_D \quad (18)$$

The detailed algorithm for training RGNN is presented in Algorithm 1.

---

#### Algorithm 1 The Training Algorithm for RGNN

---

**Require:** Training examples  $\mathbf{X}$  and  $\hat{\mathbf{Y}}$ , unlabelled testing examples  $\mathbf{X}^T$ , symmetric adjacency matrix  $\mathbf{A}$  with self-loops, learning rate  $\eta$ , number of epochs  $T$ , batch size  $B$ ;

**Ensure:** The model parameters in RGNN;

- 1: Initialize model parameters in RGNN;
- 2: **for**  $i = 1$  to  $i = T$  **do**
- 3:     **repeat**
- 4:         Draw one batch of training examples  $\mathbf{X}_B$  and  $\hat{\mathbf{Y}}_B$  from  $\mathbf{X}$  and  $\hat{\mathbf{Y}}$ , respectively; draw one batch of testing examples  $\mathbf{X}_B^T$  from  $\mathbf{X}^T$ ;
- 5:         Compute the degree matrix  $\mathbf{D}$ ;
- 6:         Compute the normalized adjacency matrix  $\mathbf{S}$ ;
- 7:         Compute the representation  $\mathbf{Z}$  in the last convolutional layer in (12);
- 8:         Use  $\mathbf{X}_B$  and  $\hat{\mathbf{Y}}_B$  to compute the KL loss  $\Phi'$  using (17);
- 9:         Use  $\mathbf{X}_B$  and  $\mathbf{X}_B^T$  to compute the domain loss  $\Phi_D$  using (13);
- 10:         Compute the GRL scaling factor  $\beta$ ;
- 11:         Update  $\mathbf{W}^D \leftarrow \mathbf{W}^D + \eta \frac{\partial \Phi_D}{\partial \mathbf{W}^D}$ ;
- 12:         Update  $\mathbf{W}^O \leftarrow \mathbf{W}^O + \eta \frac{\partial \Phi}{\partial \mathbf{W}^O}$ ;
- 13:         Update  $\mathbf{W} \leftarrow \mathbf{W} + \eta \left( \frac{\partial \Phi}{\partial \mathbf{W}} - \beta \frac{\partial \Phi_D}{\partial \mathbf{W}} \right)$ ;
- 14:         Update  $\mathbf{A} \leftarrow \mathbf{A} + \eta \left( \frac{\partial \Phi}{\partial \mathbf{A}} - \beta \frac{\partial \Phi_D}{\partial \mathbf{A}} \right)$ ;
- 15:     **until** all examples in  $\mathbf{X}$  are drawn;

---

## 5 EXPERIMENTAL SETTINGS

### 5.1 Datasets

#### 5.1.1 SEED

The SEED dataset [7] contains EEG data of 15 subjects (7 males) recorded in 62 channels using the ESI NeuroScan

System.<sup>1</sup> The EEG data is collected when participants are watching emotion-eliciting movies in three types of emotions, namely, negative, neutral and positive. Each movie lasts around 4 minutes. There are three sessions of data and each session comprises of 15 trials/movies for each subject. To make a fair comparison with existing studies, we directly use the pre-computed differential entropy (DE) features smoothed by linear dynamic systems (LDS) [7], [66] in SEED. DE extends the idea of Shannon entropy and is used to measure the complexity of a continuous random variable. For a fixed length EEG segment, DE features are computed as the logarithm energy spectrum in a certain frequency band [8]. In SEED, DE features are pre-computed over five frequency bands (delta, theta, alpha, beta and gamma) for each second of EEG signals (without overlapping) in each channel.

### 5.1.2 SEED-IV

The SEED-IV dataset [22] contains EEG data of 15 subjects (7 males) recorded in 62 channels.<sup>2</sup> The recording device is the same as the one in SEED. The EEG data is collected when participants are watching emotion-eliciting movies in four types of emotions, namely, neutral, sad, fear, and happy. Each movie lasts around 2 minutes. There are three sessions of data and each session comprises of 24 trials/movies for each subject. Similar to SEED, we use the pre-computed DE features to evaluate our model. In SEED-IV, DE features are computed over five frequency bands (delta, theta, alpha, beta and gamma) for every four second of EEG signals (without overlapping) in each channel.

## 5.2 Classification Settings

### 5.2.1 Subject-Dependent Classification

For SEED, we follow [7], [12], [17] to evaluate our RGNN model using subject-dependent classification, i.e., we evaluate our model for each subject. Specifically, for each subject, we train our model using the first 9 trials as the training set and the remaining 6 trials as the testing set. We evaluate the model performance by the average accuracy across all subjects over two sessions of EEG data in SEED. We compare our model with the following strong baselines: SVM, group sparse canonical correlation analysis (GSCCA) [67], DBN [7], spatial-temporal RNN (STRNN) [10], dynamical graph convolutional neural network (DGCNN) [12], bi-hemisphere domain adversarial neural network (BiDANN) [17], and the state-of-the-art bi-hemispheric discrepancy model (BiHDM) [13].

For SEED-IV, we follow [13], [22] to evaluate our RGNN model using subject-dependent classification. Specifically, for each subject, the first 16 trials are used for training and the remaining 8 trials containing all emotions (each emotion with two trials) are used for testing. We evaluate our model using all three sessions data. We compare our model with the following baselines: SVM, GSCCA, DBN, DGCNN, Attention LSTM (A-LSTM) [68], BiDANN, EmotionMeter [22], and BiHDM.

1. <https://compumedicsneuroscan.com/>

2. SEED-IV also contains eye movement data, which we do not use in our experiment.

### 5.2.2 Subject-Independent Classification

For SEED, we follow [12], [14], [17] to evaluate our RGNN model using subject-independent classification. We adopt leave-one-subject-out cross-validation, i.e., during each iteration, we train our model on 14 subjects and test on the remaining one subject. We evaluate the model performance by the average accuracy cross all subjects over one session of EEG data in SEED. We compare our model with the following baselines: SVM, transfer component analysis (TCA) [69], subspace alignment (SA) [70], transductive SVM (T-SVM) [71], transductive parameter transfer (TPT) [72], DGCNN, deep adaptation network (DAN) [73], BiDANN with subject adversarial training (BiDANN-S) [17], and BiHDM.

For SEED-IV, we follow [13] to evaluate our RGNN model using subject-independent classification. We evaluate our model using all three sessions data. We compare our model with the following baselines: SVM, TCA, SA, DGCNN, A-LSTM, DAN, BiDANN-S, and BiHDM.

## 5.3 Model Settings

For our RGNN in all experiments, we set the number of convolutional layers  $L = 2$ , dropout [74] rate of 0.7 at the output fully-connected layer, and batch size of 16. We use Adam optimization [75] with default  $\beta_1 = 0.9$  and  $\beta_2 = 0.999$ . We only tune the output feature dimension  $d'$ , label noise level  $\epsilon$ , learning rate  $\eta$ , L1 regularization factor  $\alpha$ , and L2 regularization for each experiment. Note that we only adopt NodeDAT in subject-independent classification experiments. The performance of all baselines is cited from published results [10], [12], [13], [17].

## 6 RESULT ANALYSIS

### 6.1 Performance Comparisons with Baselines

#### 6.1.1 Subject-Dependent Classification

Table 1 presents the subject-dependent classification accuracy (mean/standard deviation) of our RGNN model and all baselines on both SEED and SEED-IV using the pre-computed DE features. The performance on SEED using DE features across five frequency bands, namely delta, theta, alpha, beta, and gamma bands is reported as well. It is encouraging to see that our model achieves superior performance on both datasets as compared to all baselines including the state-of-the-art BiHDM when DE features from all frequency bands are used. It is worth noting that our model improves the accuracy of the state-of-the-art model on SEED-IV by nearly 5%. In particular, our model performs better than DGCNN, which is another GNN-based model that leverages the topological structure in EEG signals. Besides the proposed two regularizers, the main performance improvement can be attributed to two factors: 1) our adjacency matrix incorporates the asymmetry information between channels in left and right hemispheres; 2) our model has less concern of overfitting by extending SGC, which is much simpler than ChebNet [39] used in DGCNN.

#### 6.1.2 Subject-Independent Classification

Similar to Table 1, Table 2 presents the subject-independent classification results. When using features from all frequency bands, our model performs marginally worse than

TABLE 1: Subject-dependent classification accuracy (mean/standard deviation) on SEED and SEED-IV

Model	SEED						SEED-IV
	delta band	theta band	alpha band	beta band	gamma band	all bands	
SVM	60.50/14.14	60.95/10.20	66.64/14.41	80.76/11.56	79.56/11.38	83.99/09.92	56.61/20.05
GSCCA [67]	63.92/11.16	64.64/10.33	70.10/14.76	76.93/11.00	77.98/10.72	82.96/09.95	69.08/16.66
DBN [7]	64.32/12.45	60.77/10.42	64.01/15.97	78.92/12.48	79.19/14.58	86.08/08.34	66.77/07.38
STRNN [10]	<b>80.90/12.27</b>	<b>83.35/09.15</b>	<b>82.69/12.99</b>	83.41/10.16	69.61/15.65	89.50/07.63	-
DGCNN [12]	74.25/11.42	71.52/05.99	74.43/12.16	83.65/10.17	85.73/10.64	90.40/08.49	69.88/16.29
A-LSTM [68]	-	-	-	-	-	-	69.50/15.65
BiDANN [17]	76.97/10.95	75.56/07.88	81.03/11.74	<b>89.65/09.59</b>	88.64/09.46	92.38/07.04	70.29/12.63
EmotionMeter [22]	-	-	-	-	-	-	70.58/17.01
BiHDM [13] (SOTA)	-	-	-	-	-	93.12/06.06	74.35/14.09
RGNN (Our model)	76.17/07.91	72.26/07.25	75.33/08.85	84.25/12.54	<b>89.23/08.90</b>	<b>94.24/05.95</b>	<b>79.37/10.54</b>

TABLE 2: Subject-independent classification accuracy (mean/standard deviation) on SEED and SEED-IV

Model	SEED						SEED-IV
	delta band	theta band	alpha band	beta band	gamma band	all bands	
SVM	43.06/08.27	40.07/06.50	43.97/10.89	48.63/10.29	51.59/11.83	56.73/16.29	37.99/12.52
TCA [69]	44.10/08.22	41.26/09.21	42.93/14.33	43.93/10.06	48.43/09.73	63.64/14.88	56.56/13.77
SA [70]	53.23/07.47	50.60/08.31	55.06/10.60	56.72/10.78	64.47/14.96	69.00/10.89	64.44/09.46
T-SVM [71]	-	-	-	-	-	72.53/14.00	-
TPT [72]	-	-	-	-	-	76.31/15.89	-
DGCNN [12]	49.79/10.94	46.36/12.06	48.29/12.28	56.15/14.01	54.87/17.53	79.95/09.02	52.82/09.23
A-LSTM [68]	-	-	-	-	-	-	55.03/09.28
DAN [73]	-	-	-	-	-	83.81/08.56	58.87/08.13
BiDANN-S [17]	63.01/07.49	<b>63.22/07.52</b>	<b>63.50/09.50</b>	73.59/09.12	73.72/08.67	84.14/06.87	65.59/10.39
BiHDM [13] (SOTA)	-	-	-	-	-	<b>85.40/07.53</b>	69.03/08.66
RGNN (Our model)	<b>64.88/06.87</b>	60.69/05.79	60.84/07.57	<b>74.96/08.94</b>	<b>77.50/08.10</b>	85.30/06.72	<b>73.84/08.02</b>

BiHDM on SEED but much better than BiHDM on SEED-IV. In addition, our model achieves the lowest standard deviation in accuracy compared to all baselines on both datasets, demonstrating the robustness of our model. Comparing the numbers in both Table 1 and 2, we find that the accuracy obtained in subject-independent settings is consistently worse than the accuracy obtained in subject-dependent settings by around 5% to 30% for each model. This finding is unsurprising because the variability of EEG signals across subjects makes subject-independent classification more challenging. However, the interesting part is that the performance gap between these two settings is gradually decreasing from around 27% on SEED and 19% on SEED-IV using SVM to around 9% on SEED and 6% on SEED-IV using our model. One possible reason for the diminishing gap is that recent deep learning models in subject-independent settings are becoming better at leveraging the larger amount of data and learning more subject-invariant EEG representations. This observation seems to indicate that transfer learning may be a very important tool for emotion recognition in cross-subject settings. With the increasing amount of data available from different subjects and a proper transfer learning tool, it would not be surprising that subject-independent classification accuracy will surpass the subject-dependent classification accuracy.

### 6.1.3 Performance Comparison of Frequency Bands

We compare the performance of our model and all baselines using features from different frequency bands. For SEED, the results are reported in Table 1 and 2. In subject-dependent experiments on SEED, STRNN achieves the highest accuracy in delta, theta and alpha bands, BiDANN performs the best in beta band, and our model performs the best in gamma band. In subject-independent experiments

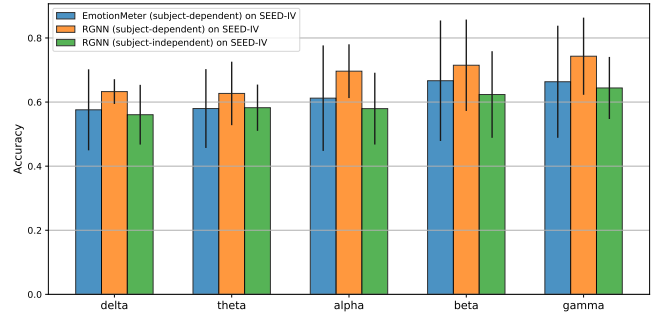


Fig. 3: Subject-dependent classification accuracy for EmotionMeter and RGNN, and subject-independent classification accuracy for RGNN across five frequency bands on SEED-IV

on SEED, BiDANN-S achieves the highest accuracy in theta and alpha bands, and our model performs the best in delta, beta and gamma bands. For SEED-IV, the results are illustrated in Figure 3. Note that the subject-independent results for EmotionMeter are not available. It is clear that our model consistently performs better than EmotionMeter in all frequency bands.

We investigate the critical frequency bands for emotion recognition. For both subject-dependent and subject-independent settings on both datasets, we compare the performance of each model across different frequency bands. In general, most models including our model achieve better performance on beta and gamma bands than delta, theta and alpha bands, with one exception of STRNN, which performs the worst on gamma band. This observation is consistent with the literature [7], [76]. Our model performs

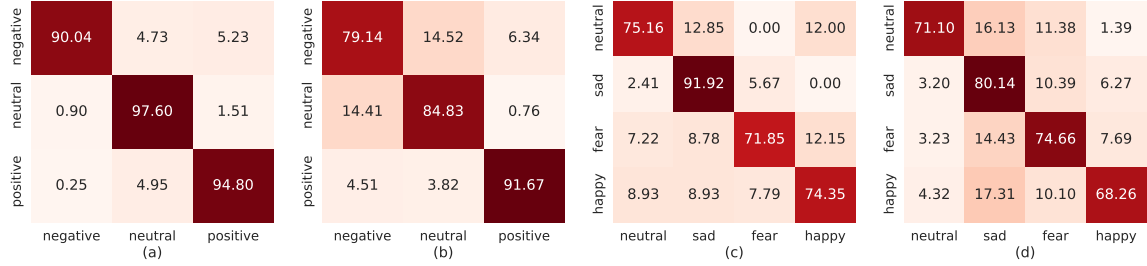


Fig. 4: Confusion matrix of RGNN. (a) subject-dependent classification on SEED. (b) subject-independent classification on SEED. (c) subject-dependent classification on SEED-IV. (d) subject-independent classification on SEED-IV.

TABLE 3: Ablation study for subject-independent classification accuracy (mean/standard deviation) on SEED and SEED-IV

Model	SEED	SEED-IV
RGNN	<b>85.30/06.72</b>	<b>73.84/08.02</b>
- global connection	82.42/08.24	71.13/08.78
- symmetric adjacency matrix	83.69/07.92	72.02/08.66
- NodeDAT	81.92/09.35	71.65/09.43
- NodeDAT + DAT	83.51/08.11	72.40/08.54
- EmotionDL	82.27/08.81	70.76/09.22

consistently better in gamma band than beta band and the rest three bands, indicating that gamma band may be the most discriminative band for our model.

#### 6.1.4 Confusion Matrix

We present the confusion matrix of our model in Figure 4. For both subject-dependent and subject-independent settings on SEED, our model can recognize more happy and neutral emotions than sad. By combining training data from other subjects, our model is getting much worse at detecting sad emotion, indicating that participants are likely to generate very different EEG patterns when experiencing sad emotion. This phenomenon can be observed in SEED-IV as well. For SEED-IV, our model performs the significantly better on sad emotion than all other emotions in both classification settings. We notice that fear is the only emotion that performs better in subject-independent classification than subject-dependent classification. This finding indicates that participants watching horror movies may generate similar EEG patterns.

## 6.2 Model Analysis

### 6.2.1 Ablation Study

We conduct ablation study to investigate the contribution of each key component in our model. The results are obtained in subject-independent setting on both datasets, as reported in Table 3. The two major designs in our adjacency matrix A, i.e., global connection and symmetric adjacency matrix design, are helpful in recognizing emotions. The global connection models the asymmetric difference between neuronal activities in the left and right hemispheres and have been shown to reveal certain emotions [5], [61], [62]. The symmetric adjacency matrix design is mostly motivated to prevent overfitting, especially in subject-dependent classifications where less training data is available.

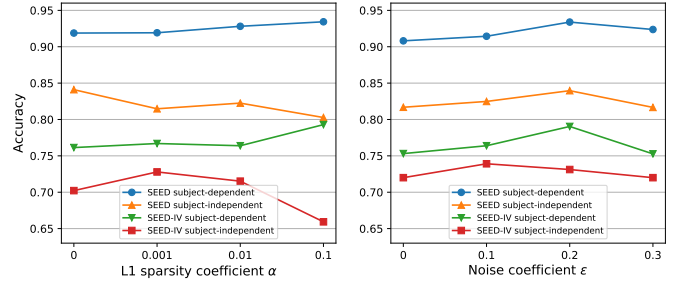


Fig. 5: Classification accuracy of RGNN with varying L1 sparsity coefficient  $\alpha$  in (11) and noise coefficient  $\epsilon$  in (15) and (16)

Our NodeDAT has a noticeable positive impact on our model performance, which demonstrates that domain adaptation is very helpful for cross-subject classification. To further investigate the impact of our node-level domain classifier, we further experimented with replacing our NodeDAT by a generic domain classifier (DAT) [20] that operates after the pooling operation, i.e., the row with (-NodeDAT + DAT). The clear performance gap between (-NodeDAT + DAT) and our RGNN model indicates that our NodeDAT can better regularize the model by learning subject-invariant representation at node level than graph level. In addition, by removing NodeDAT, the performance of our model has a greater variance, demonstrating the importance of NodeDAT in improving the robustness of our model against cross-subject variations.

Our EmotionDL improves our model performance by around 3% in accuracy on both datasets. This performance gain validates our assumption that participants are not always generating the intended emotions when watching emotion-eliciting movies. In addition, our EmotionDL can be easily implemented into other deep learning models.

### 6.2.2 Sensitivity Analysis

We analyze the performance of our model across varying L1 sparsity coefficient  $\alpha$  (see (11)) and noise coefficient  $\epsilon$  in EmotionDL (see (15) and (16)), as illustrated in Figure 5. For subject-dependent classification, increasing  $\alpha$  from 0 to 0.1 will generally increase the model performance. However, for subject-independent classification, increasing  $\alpha$  beyond a threshold will decrease the model performance. One possible explanation for the difference in model behaviors is that there is much less training data in subject-dependent

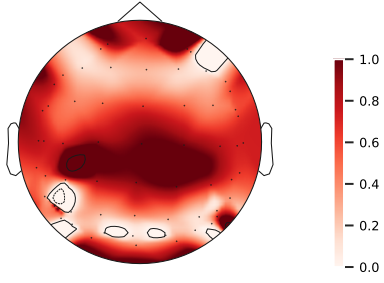


Fig. 6: Heatmap of the diagonal values in the learned adjacency matrix  $\mathbf{A}$ , which is averaged across five frequency bands in subject-dependent classification on both SEED and SEED-IV.

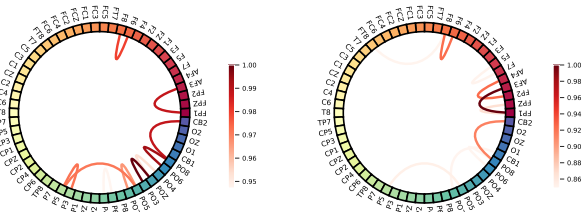


Fig. 7: Top 10 edge weights between electrodes in the adjacency matrix  $\mathbf{A}$  (excluding global connections in (10) for better clarity). Left figure: when  $\mathbf{A}$  is initialized. Right figure: when  $\mathbf{A}$  is learned and averaged across five frequency bands in subject-dependent classification on both SEED and SEED-IV.

classification, which thus requires a stronger regularization to reduce overfitting, whereas for subject-independent classification where training data is abundant, adding strong regularization may introduce bias and hinder the learning of our model.

As illustrated in Figure 5 (right), our model behaves consistently across different experimental settings with varying noise coefficient  $\epsilon$ . Specifically, the performance of our model first increases and then decreases with increasing  $\epsilon$ . In particular, our model usually performs the best when  $\epsilon$  is around 0.2. Introducing excessive noise causes performance drop, which is expected because excessive noise weakens the true learning signals.

### 6.3 Neuronal Activities for Emotion Recognition

#### 6.3.1 Activation Maps of Channels

Figure 6 plots the heatmap of the diagonal elements in our learned adjacency matrix  $\mathbf{A}$ , which is averaged across all frequency bands in subject-dependent classification on both SEED and SEED-IV. The values for each channel is further normalized to the  $[0, 1]$  interval for better visualization. Conceptually, as shown in (4), the diagonal values in  $\mathbf{A}$  represents the contribution of each channel in computing the final EEG representation. It is clear that there are strong

activations on the pre-frontal, parietal, and occipital regions, indicating that these regions may be strongly related to the emotion processing of the brain. Our finding is consistent with existing studies which observed that asymmetrical frontal and parietal EEG activity may reflect changes on both valence and arousal [5], [77]. The synchronization between frontal and occipital region has also been reported to be related to positive and fear emotion [78], [79]. The clear asymmetry pattern on the activation map of channels indicate again that the asymmetry in EEG activity between left and right hemisphere are critical for emotion recognition.

#### 6.3.2 Inter-channel Relations

Figure 7 plots the top 10 connections between channels having the largest edge weight in our adjacency matrix  $\mathbf{A}$ . Figure 7 (left) is plotted when  $\mathbf{A}$  is initialized as in (9). Figure 7 (right) is plotted when  $\mathbf{A}$  is learned and averaged across five frequency bands in subject-dependent classification on both SEED and SEED-IV. We removed global connections introduced in (10) in our plots for better clarity. Note that all global connections remain among the strongest connections after  $\mathbf{A}$  is learned, demonstrating again that global connections are essential for emotion recognition. It is clear from Figure 7 that there are some similarities and differences between these two plots, indicating that our initialization strategy in (9) can capture local inter-channel relations to a certain degree. One notable difference between the two plots is that a few strong connections in Figure 7 (left) is gone, e.g., (POZ, PO3), (PO6, PO8), and (P3, P5), indicating that these connections may not be critical for emotion recognition. In addition, it is clear from Figure 7 (right) that the connection between the channel pair (FP1, AF3) is the strongest, followed by (F6, F8), (FP2, AF4), and (PO8, CB2), indicating that local inter-channel relations in the frontal region may be important for emotion recognition.

## 7 CONCLUSION

In this paper, we propose a regularized graph neural network for emotion recognition based on EEG signals. Our model is biologically supported to capture both local and global inter-channel relations. In addition, we propose two regularizers, namely NodeDAT and EmotionDL, to improve the robustness of our model against cross-subject EEG variations and noisy labels. We evaluate our model in both subject-dependent and subject-independent classification settings on two public datasets SEED and SEED-IV. Our model obtains better performance than a few competitive baselines such as SVM, DBN, DGCNN, BiDANN, and the state-of-the-art BiHDM on most of the tasks. Notably, our model achieves accuracy of 79.37% and 73.84% in subject-dependent and subject-independent classifications on SEED-IV, respectively, outperforming the current state-of-the-art model by around 5%. Our model analysis demonstrate that our proposed biologically-supported adjacency matrix and two regularizers contribute consistent and significant gain to the performance of our model. Investigations on the neuronal activities reveal that pre-frontal, parietal and occipital regions may be the most informative regions in emotion recognition. In addition, local inter-channel relations between (FP1, AF3), (F6, F8) and (FP2, AF4) may provide useful information as well.

In the future, we plan to investigate how to apply our model to EEG signals that have a smaller number of channels. The smaller number of nodes or channels in the graph simplifies the graph convolution operation in our model. A simpler version of our model may be necessary to avoid overfitting on these datasets. In addition, how to incorporate global connections on these smaller graphs may be worth exploring.

## REFERENCES

- [1] S. M. Alarcao and M. J. Fonseca, "Emotions recognition using eeg signals: a survey," *IEEE Transactions on Affective Computing*, 2017.
- [2] U. R. Acharya, V. K. Sudarshan, H. Adeli, J. Santhosh, J. E. Koh, and A. Adeli, "Computer-aided diagnosis of depression using eeg signals," *European neurology*, vol. 73, no. 5-6, pp. 329–336, 2015.
- [3] P. Ekman and D. Keltner, "Universal facial expressions of emotion," *Segerstrale U, P. Molnar P, eds. Nonverbal communication: Where nature meets culture*, pp. 27–46, 1997.
- [4] A. Mehrabian, "Pleasure-arousal-dominance: A general framework for describing and measuring individual differences in temperament," *Current Psychology*, vol. 14, no. 4, pp. 261–292, 1996.
- [5] L. A. Schmidt and L. J. Trainor, "Frontal brain electrical activity (eeg) distinguishes valence and intensity of musical emotions," *Cognition & Emotion*, vol. 15, no. 4, pp. 487–500, 2001.
- [6] X.-W. Wang, D. Nie, and B.-L. Lu, "Emotional state classification from eeg data using machine learning approach," *Neurocomputing*, vol. 129, pp. 94–106, 2014.
- [7] W.-L. Zheng and B.-L. Lu, "Investigating critical frequency bands and channels for eeg-based emotion recognition with deep neural networks," *IEEE Transactions on Autonomous Mental Development*, vol. 7, no. 3, pp. 162–175, 2015.
- [8] L.-C. Shi, Y.-Y. Jiao, and B.-L. Lu, "Differential entropy feature for eeg-based vigilance estimation," in *2013 35th Annual International Conference of the IEEE Engineering in Medicine and Biology Society (EMBC)*. IEEE, 2013, pp. 6627–6630.
- [9] D. Zhang, L. Yao, X. Zhang, S. Wang, W. Chen, R. Boots, and B. Bejnatallah, "Cascade and parallel convolutional recurrent neural networks on eeg-based intention recognition for brain computer interface," in *Thirty-Second AAAI Conference on Artificial Intelligence*, 2018.
- [10] T. Zhang, W. Zheng, Z. Cui, Y. Zong, and Y. Li, "Spatial-temporal recurrent neural network for emotion recognition," *IEEE transactions on cybernetics*, no. 99, pp. 1–9, 2018.
- [11] R. Pascanu, T. Mikolov, and Y. Bengio, "On the difficulty of training recurrent neural networks," in *International conference on machine learning*, 2013, pp. 1310–1318.
- [12] T. Song, W. Zheng, P. Song, and Z. Cui, "Eeg emotion recognition using dynamical graph convolutional neural networks," *IEEE Transactions on Affective Computing*, 2018.
- [13] Y. Li, W. Zheng, L. Wang, Y. Zong, L. Qi, Z. Cui, T. Zhang, and T. Song, "A novel bi-hemispheric discrepancy model for eeg emotion recognition," *arXiv preprint arXiv:1906.01704*, 2019.
- [14] W.-L. Zheng and B.-L. Lu, "Personalizing eeg-based affective models with transfer learning," in *Proceedings of the Twenty-Fifth International Joint Conference on Artificial Intelligence*. AAAI Press, 2016, pp. 2732–2738.
- [15] X. Chai, Q. Wang, Y. Zhao, Y. Li, D. Liu, X. Liu, and O. Bai, "A fast, efficient domain adaptation technique for cross-domain electroencephalography (eeg)-based emotion recognition," *Sensors*, vol. 17, no. 5, p. 1014, 2017.
- [16] Z. Lan, O. Sourina, L. Wang, R. Scherer, and G. R. Müller-Putz, "Domain adaptation techniques for eeg-based emotion recognition: a comparative study on two public datasets," *IEEE Transactions on Cognitive and Developmental Systems*, vol. 11, no. 1, pp. 85–94, 2018.
- [17] Y. Li, W. Zheng, Y. Zong, Z. Cui, T. Zhang, and X. Zhou, "A bi-hemisphere domain adversarial neural network model for eeg emotion recognition," *IEEE Transactions on Affective Computing*, 2018.
- [18] E. Bullmore and O. Sporns, "The economy of brain network organization," *Nature Reviews Neuroscience*, vol. 13, no. 5, p. 336, 2012.
- [19] F. Wu, A. Souza, T. Zhang, C. Fifty, T. Yu, and K. Weinberger, "Simplifying graph convolutional networks," in *Proceedings of the 36th International Conference on Machine Learning*. PMLR, 2019, pp. 6861–6871.
- [20] Y. Ganin, E. Ustinova, H. Ajakan, P. Germain, H. Larochelle, F. Laviolette, M. Marchand, and V. Lempitsky, "Domain-adversarial training of neural networks," *The Journal of Machine Learning Research*, vol. 17, no. 1, pp. 2096–2030, 2016.
- [21] X. Zhu and X. Wu, "Class noise vs. attribute noise: A quantitative study," *Artificial intelligence review*, vol. 22, no. 3, pp. 177–210, 2004.
- [22] W.-L. Zheng, W. Liu, Y. Lu, B.-L. Lu, and A. Cichocki, "Emotionmeter: A multimodal framework for recognizing human emotions," *IEEE transactions on cybernetics*, no. 99, pp. 1–13, 2018.
- [23] K. Takahashi and A. Tsukaguchi, "Remarks on emotion recognition from multi-modal bio-potential signals," in *SMC'03 Conference Proceedings. 2003 IEEE International Conference on Systems, Man and Cybernetics. Conference Theme-System Security and Assurance (Cat. No. 03CH37483)*, vol. 2. IEEE, 2003, pp. 1654–1659.
- [24] B. Hjorth, "Eeg analysis based on time domain properties," *Electroencephalography and clinical neurophysiology*, vol. 29, no. 3, pp. 306–310, 1970.
- [25] Y. Liu and O. Sourina, "Real-time fractal-based valence level recognition from eeg," in *Transactions on computational science XVIII*. Springer, 2013, pp. 101–120.
- [26] M. Akin, "Comparison of wavelet transform and fft methods in the analysis of eeg signals," *Journal of medical systems*, vol. 26, no. 3, pp. 241–247, 2002.
- [27] R. Jenke, A. Peer, and M. Buss, "Feature extraction and selection for emotion recognition from eeg," *IEEE Transactions on Affective Computing*, vol. 5, no. 3, pp. 327–339, 2014.
- [28] X. Wu, W.-L. Zheng, and B.-L. Lu, "Identifying functional brain connectivity patterns for eeg-based emotion recognition," in *2019 9th International IEEE/EMBS Conference on Neural Engineering (NER)*. IEEE, 2019, pp. 235–238.
- [29] P. Li, H. Liu, Y. Si, C. Li, F. Li, X. Zhu, X. Huang, Y. Zeng, D. Yao, Y. Zhang *et al.*, "Eeg based emotion recognition by combining functional connectivity network and local activations," *IEEE Transactions on Biomedical Engineering*, 2019.
- [30] W.-L. Zheng, J.-Y. Zhu, Y. Peng, and B.-L. Lu, "Eeg-based emotion classification using deep belief networks," in *2014 IEEE International Conference on Multimedia and Expo (ICME)*. IEEE, 2014, pp. 1–6.
- [31] B. H. Kim and S. Jo, "Deep physiological affect network for the recognition of human emotions," *IEEE Transactions on Affective Computing*, 2018.
- [32] P. Bashivan, I. Rish, M. Yeasin, and N. Codella, "Learning representations from eeg with deep recurrent-convolutional neural networks," *arXiv preprint arXiv:1511.06448*, 2015.
- [33] X. Li, D. Song, P. Zhang, G. Yu, Y. Hou, and B. Hu, "Emotion recognition from multi-channel eeg data through convolutional recurrent neural network," in *2016 IEEE International Conference on Bioinformatics and Biomedicine (BIBM)*. IEEE, 2016, pp. 352–359.
- [34] J. Li, Z. Zhang, and H. He, "Hierarchical convolutional neural networks for eeg-based emotion recognition," *Cognitive Computation*, pp. 1–13, 2018.
- [35] Z. Wu, S. Pan, F. Chen, G. Long, C. Zhang, and P. S. Yu, "A comprehensive survey on graph neural networks," *arXiv preprint arXiv:1901.00596*, 2019.
- [36] F. Scarselli, M. Gori, A. C. Tsoi, M. Hagenbuchner, and G. Monfardini, "The graph neural network model," *IEEE Transactions on Neural Networks*, vol. 20, no. 1, pp. 61–80, 2008.
- [37] J. Bruna, W. Zaremba, A. Szlam, and Y. LeCun, "Spectral networks and locally connected networks on graphs," *arXiv preprint arXiv:1312.6203*, 2013.
- [38] F. R. Chung and F. C. Graham, *Spectral graph theory*. American Mathematical Soc., 1997, no. 92.
- [39] M. Defferrard, X. Bresson, and P. Vandergheynst, "Convolutional neural networks on graphs with fast localized spectral filtering," in *Advances in neural information processing systems*, 2016, pp. 3844–3852.
- [40] T. N. Kipf and M. Welling, "Semi-supervised classification with graph convolutional networks," in *International Conference on Learning Representations (ICLR)*, 2017.
- [41] P. Velikovi, G. Cucurull, A. Casanova, A. Romero, P. Li, and Y. Bengio, "Graph attention networks," in *International Conference on Learning Representations*, 2018. [Online]. Available: <https://openreview.net/forum?id=rJXMpikCZ>

- [42] A. Vaswani, N. Shazeer, N. Parmar, J. Uszkoreit, L. Jones, A. N. Gomez, Ł. Kaiser, and I. Polosukhin, "Attention is all you need," in *Advances in neural information processing systems*, 2017, pp. 5998–6008.
- [43] Y. Li, D. Tarlow, M. Brockschmidt, and R. Zemel, "Gated graph sequence neural networks," *arXiv preprint arXiv:1511.05493*, 2015.
- [44] K. Cho, B. van Merriënboer, C. Gulcehre, D. Bahdanau, F. Bougares, H. Schwenk, and Y. Bengio, "Learning phrase representations using RNN encoder–decoder for statistical machine translation," in *Proceedings of the 2014 Conference on Empirical Methods in Natural Language Processing (EMNLP)*. Association for Computational Linguistics, 2014, pp. 1724–1734.
- [45] J. Zhou, G. Cui, Z. Zhang, C. Yang, Z. Liu, and M. Sun, "Graph neural networks: A review of methods and applications," *arXiv preprint arXiv:1812.08434*, 2018.
- [46] J. Huang, A. Gretton, K. Borgwardt, B. Schölkopf, and A. J. Smola, "Correcting sample selection bias by unlabeled data," in *Advances in neural information processing systems*, 2007, pp. 601–608.
- [47] A. Gretton, K. M. Borgwardt, M. J. Rasch, B. Schölkopf, and A. Smola, "A kernel two-sample test," *Journal of Machine Learning Research*, vol. 13, no. Mar, pp. 723–773, 2012.
- [48] M. Ghifary, W. B. Kleijn, M. Zhang, D. Balduzzi, and W. Li, "Deep reconstruction-classification networks for unsupervised domain adaptation," in *European Conference on Computer Vision*. Springer, 2016, pp. 597–613.
- [49] S. Benaim and L. Wolf, "One-sided unsupervised domain mapping," in *Advances in neural information processing systems*, 2017, pp. 752–762.
- [50] F. M. Cariucci, L. Porzi, B. Caputo, E. Ricci, and S. R. Bulò, "Autodial: Automatic domain alignment layers," in *2017 IEEE International Conference on Computer Vision (ICCV)*. IEEE, 2017, pp. 5077–5085.
- [51] G. Wilson and D. J. Cook, "A Survey of Unsupervised Deep Domain Adaptation," *arXiv e-prints*, p. arXiv:1812.02849, Dec 2018.
- [52] L. Zhang, "Transfer adaptation learning: A decade survey," *CoRR*, vol. abs/1903.04687, 2019. [Online]. Available: <http://arxiv.org/abs/1903.04687>
- [53] G. Patrini, A. Rozza, A. Krishna Menon, R. Nock, and L. Qu, "Making deep neural networks robust to label noise: A loss correction approach," in *Proceedings of the IEEE Conference on Computer Vision and Pattern Recognition*, 2017, pp. 1944–1952.
- [54] S. Sukhbaatar, J. Bruna, M. Paluri, L. Bourdev, and R. Fergus, "Training convolutional networks with noisy labels," *arXiv preprint arXiv:1406.2080*, 2014.
- [55] B. Van Rooyen, A. Menon, and R. C. Williamson, "Learning with symmetric label noise: The importance of being unhinged," in *Advances in Neural Information Processing Systems*, 2015, pp. 10–18.
- [56] J. P. Brooks, "Support vector machines with the ramp loss and the hard margin loss," *Operations research*, vol. 59, no. 2, pp. 467–479, 2011.
- [57] S. Reed, H. Lee, D. Anguelov, C. Szegedy, D. Erhan, and A. Rabinovich, "Training deep neural networks on noisy labels with bootstrapping," *arXiv preprint arXiv:1412.6596*, 2014.
- [58] D. Tanaka, D. Ikami, T. Yamasaki, and K. Aizawa, "Joint optimization framework for learning with noisy labels," in *Proceedings of the IEEE Conference on Computer Vision and Pattern Recognition*, 2018, pp. 5552–5560.
- [59] B.-B. Gao, C. Xing, C.-W. Xie, J. Wu, and X. Geng, "Deep label distribution learning with label ambiguity," *IEEE Transactions on Image Processing*, vol. 26, no. 6, pp. 2825–2838, 2017.
- [60] R. Salvador, J. Suckling, M. R. Coleman, J. D. Pickard, D. Menon, and E. Bullmore, "Neurophysiological architecture of functional magnetic resonance images of human brain," *Cerebral cortex*, vol. 15, no. 9, pp. 1332–1342, 2005.
- [61] S. J. Dimond, L. Farrington, and P. Johnson, "Differing emotional response from right and left hemispheres," *Nature*, vol. 261, no. 5562, p. 690, 1976.
- [62] G. Zhao, Y. Zhang, and Y. Ge, "Frontal eeg asymmetry and middle line power difference in discrete emotions," *Frontiers in behavioral neuroscience*, vol. 12, 2018.
- [63] S. Achard and E. Bullmore, "Efficiency and cost of economical brain functional networks," *PLoS computational biology*, vol. 3, no. 2, p. e17, 2007.
- [64] K. Xu, W. Hu, J. Leskovec, and S. Jegelka, "How powerful are graph neural networks?" in *International Conference on Learning Representations*, 2019. [Online]. Available: <https://openreview.net/forum?id=ryGs6iA5Km>
- [65] S. Kullback and R. A. Leibler, "On information and sufficiency," *The annals of mathematical statistics*, vol. 22, no. 1, pp. 79–86, 1951.
- [66] L.-C. Shi and B.-L. Lu, "Off-line and on-line vigilance estimation based on linear dynamical system and manifold learning," in *2010 Annual International Conference of the IEEE Engineering in Medicine and Biology*. IEEE, 2010, pp. 6587–6590.
- [67] W. Zheng, "Multichannel eeg-based emotion recognition via group sparse canonical correlation analysis," *IEEE Transactions on Cognitive and Developmental Systems*, vol. 9, no. 3, pp. 281–290, 2016.
- [68] T. Song, W. Zheng, C. Lu, Y. Zong, X. Zhang, and Z. Cui, "Mped: A multi-modal physiological emotion database for discrete emotion recognition," *IEEE Access*, vol. 7, pp. 12 177–12 191, 2019.
- [69] S. J. Pan, I. W. Tsang, J. T. Kwok, and Q. Yang, "Domain adaptation via transfer component analysis," *IEEE Transactions on Neural Networks*, vol. 22, no. 2, pp. 199–210, 2010.
- [70] B. Fernando, A. Habrard, M. Sebban, and T. Tuytelaars, "Unsupervised visual domain adaptation using subspace alignment," in *Proceedings of the IEEE international conference on computer vision*, 2013, pp. 2960–2967.
- [71] R. Collobert, F. Sinz, J. Weston, and L. Bottou, "Large scale transductive svms," *Journal of Machine Learning Research*, vol. 7, no. Aug, pp. 1687–1712, 2006.
- [72] E. Sangineto, G. Zen, E. Ricci, and N. Sebe, "We are not all equal: Personalizing models for facial expression analysis with transductive parameter transfer," in *Proceedings of the 22nd ACM international conference on Multimedia*. ACM, 2014, pp. 357–366.
- [73] H. Li, Y.-M. Jin, W.-L. Zheng, and B.-L. Lu, "Cross-subject emotion recognition using deep adaptation networks," in *International Conference on Neural Information Processing*. Springer, 2018, pp. 403–413.
- [74] N. Srivastava, G. Hinton, A. Krizhevsky, I. Sutskever, and R. Salakhutdinov, "Dropout: a simple way to prevent neural networks from overfitting," *The journal of machine learning research*, vol. 15, no. 1, pp. 1929–1958, 2014.
- [75] D. P. Kingma and J. Ba, "Adam: A method for stochastic optimization," *arXiv preprint arXiv:1412.6980*, 2014.
- [76] W. J. Ray and H. W. Cole, "Eeg alpha activity reflects attentional demands, and beta activity reflects emotional and cognitive processes," *Science*, vol. 228, no. 4700, pp. 750–752, 1985.
- [77] Y.-P. Lin, C.-H. Wang, T.-P. Jung, T.-L. Wu, S.-K. Jeng, J.-R. Duann, and J.-H. Chen, "Eeg-based emotion recognition in music listening," *IEEE Transactions on Biomedical Engineering*, vol. 57, no. 7, pp. 1798–1806, 2010.
- [78] T. Costa, E. Rognoni, and D. Galati, "Eeg phase synchronization during emotional response to positive and negative film stimuli," *Neuroscience letters*, vol. 406, no. 3, pp. 159–164, 2006.
- [79] G. Mattavelli, M. Rosanova, A. G. Casali, C. Papagno, and L. J. R. Lauro, "Timing of emotion representation in right and left occipital region: evidence from combined tms-eeg," *Brain and cognition*, vol. 106, pp. 13–22, 2016.